RSC Advances

PAPER

View Article Online
View Journal | View Issue

Cite this: *RSC Adv.*, 2017, **7**, 22121

Fabrication of nanostructures through self-assembly of non-ionic amphiphiles for biomedical applications†

Suchita Prasad,[a] Katharina Achazi,[b] Christoph Böttcher,[c] Rainer Haag*[b] and Sunil K. Sharma*[a]

Fabrication of self-assembled nanostructures with defined size and morphology represents a formidable challenge and thus, has gained tremendous momentum in research because of their potential applications in various biological systems. Herein, we report on the synthesis of novel non-ionic amphiphiles using 2,2-di(prop-2-yn-1-yl)propane-1,3-diol as a core further functionalized with poly(ethylene glycol) monomethyl ether and alkyl chains employing a chemo-enzymatic approach. Surface tension and fluorescence measurements along with dynamic light scattering studies revealed that all of the amphiphilic systems spontaneously self-assemble in aqueous solution, which is further supplemented by cryogenic transmission electron microscopy. The solubilization behavior of these systems as evidenced from UV-Vis and fluorescence spectroscopy and high performance liquid chromatography suggested the effective encapsulation of hydrophobic entities like Nile red, nimodipine, curcumin and dexamethasone. A comparative study with a standard excipient, Cremophor® ELP demonstrated that our nanocarriers exhibited superior/equivalent solubilization behavior for curcumin. Confocal laser scanning microscopy revealed efficient uptake of encapsulated dye in the cytosol of lung cancer cells, thus suggesting, that the reported amphiphilic systems can transport drugs into cells. A study of cytotoxicity showed that the synthesized amphiphilic systems are non-cytotoxic at the concentrations studied. The release profile of encapsulated Nile red incubated with/without a hydrolase enzyme *Candida antarctica* lipase demonstrated that the dye is stable in the amphiphilic nanostructures in the absence of enzyme for up to 12 days, however, more than 90% release of the dye occurred in 12 days when incubated with lipase. The results advocate the potential of these nanostructures as prospective drug delivery vehicles.

Received 24th December 2016
Accepted 4th April 2017

DOI: 10.1039/c6ra28654b

rsc.li/rsc-advances

1. Introduction

The self-assembling behavior of molecular building blocks (lipids, carbohydrates, proteins and nucleic acids) to generate structurally precise and functional supramolecular architectures, driven by various non-covalent interactions such as hydrophobic, ionic, π–π stacking and hydrogen bonding, outlines the essence of life on earth.[1–5] This has prompted the sophisticated fabrication of an array of structurally diverse and functional nano-structured materials to open up newer avenues for biomedical and bio-nanotechnological applications.[6–10] Among the diverse and myriad promising applications offered by these architectures, the area of drug delivery is of colossal importance as more than 80% of drugs are small molecules that diffuse rapidly all over the body without selectivity because of their tendency to interact through multiple binding sites, leading to undesired side-effects.[11] Confronted with the challenges of drug delivery such as low aqueous solubility of drugs, short half-life in the bloodstream and high drug dosage, concomitant with the adverse effects associated with the current solubilizers used,[12–14] research on biocompatible nano-scale drug delivery vehicles which are indispensable to mediate target specific deployment of drugs, holds substantial promise.

Among the many nano-structured drug delivery vehicles being studied, amphiphilic architectures have garnered considerable attention, which stems from the extensive research in this field. Amphiphiles, delineated by dual binding affinity, self-assemble as a consequence of the interplay of hydrophobic and hydrophilic molecular domains in an aqueous environment to achieve a state of minimum free energy, leading to the formation of wide range of morphologies.[15–17] Harnessing

[a]*Department of Chemistry, University of Delhi, Delhi 110 007, India. E-mail: sksharma@chemistry.du.ac.in; Tel: +91-11-27666646*

[b]*Institut für Chemie und Biochemie, Freie Universität Berlin, Takustraße 3, 14195 Berlin, Germany. E-mail: haag@zedat.fu-berlin.de; Fax: +49-30-838-452633; Tel: +49-30-838-52633*

[c]*Forschungszentrum für Elektronenmikroskopie, Institut für Chemie und Biochemie, Freie Universität Berlin, Fabeckstraße 36a, 14195 Berlin, Germany*

† Electronic supplementary information (ESI) available. See DOI: 10.1039/c6ra28654b

the potential of supramolecular assemblies of amphiphiles requires playing with the experimental variables together with engineering over their chemical, structural and functional properties.[17] Endowed with an internal cavity, these can be successfully exploited for the delivery of active components.[18,19]

Though the amphiphilic nanocarriers can be either ionic or non-ionic, however, the latter have emanated as potential biomedical candidates and have witnessed tremendous research due to the limitations experienced by the ionic counterparts, particularly the cationic one.[11,20] Gemini surfactants, characterized by the presence of two hydrophilic head groups and two hydrophobic tails, linked by a rigid or flexible spacer, holds unique properties and rich self-assembly behaviour, as a result of which they have gained considerable attention.[21,22] Fabricating these dimeric or twin amphiphiles confers them superior physico-chemical properties compared to the conventional monomeric surfactants *e.g.* low critical micellar concentration (CMC) as a consequence of the presence of two hydrophobic tails, high surface activity, high solubilization capacity, low Krafft temperature, unusual rheological properties, multiple aggregate morphologies, high wetting ability *etc.*[23,24] The micellar assembly formed by Gemini surfactants seem adequate as long circulating drug carriers, owing to the much lower CMC values and longer micellar lifetimes.[25] The above factors make Gemini amphiphiles of special interest for biomedical applications.

In an endeavor to create novel non-ionic Gemini amphiphilic constructs having tailored structure, fashioned with suitable functionalities, we used 2,2-di(prop-2-yn-1-yl)propane-1,3-diol as the core unit. The diol was successfully grafted with alkyl chains and biocompatible poly(ethylene glycol) monomethyl ether (mPEG) of variable lengths to confer hydrophobicity and hydrophilicity, respectively and studied their effect on transport capacities. A bunch of literature reports reveals that 2,2-di(prop-2-yn-1-yl)propane-1,3-diol has been successfully used as a component for metathesis cyclopolymerization.[26–33] In contrast, there are only two reports wherein the diol has been utilized to afford low-molecular weight amphiphilic molecules. Das *et al.* initiated the synthesis of thiophene-capped cyclopenta[*c*]thiophene, further functionalized with carbohydrate using the diol for Concanavalin A (protein isolated from jack bean) recognition.[34] Further, the diol has been exploited for the synthesis of Y-shaped sugar-based surfactants by Ali and co-workers and have been studied for their lyotropic and surface properties.[35] However, this is for the first time that 2,2-di(prop-2-yn-1-yl)propane-1,3-diol has been incorporated as a core along with mPEG as hydrophilic moiety to accomplish the synthesis of Gemini amphiphiles, which have been further investigated for their transport behavior using model dyes/drugs. In pursuit of enhanced stability of supramolecular assemblies and solubility of hydrophobic guest molecules,[36] aromatic units have been introduced. The synthesized amphiphiles were studied for their supramolecular aggregation behavior by dynamic light scattering (DLS), surface tension and fluorescence measurements using 'pyrene' and 'Nile red' as probes. The aggregation tendency of the amphiphilic molecules was further augmented by cryogenic transmission electron microscopy (cryo-TEM). The cytotoxicity profile of all the resulting amphiphilic architectures was evaluated using A549 cells (adenocarcinomic human alveolar basal epithelial cells). Furthermore, the amphiphiles synthesized were explored for their transport potential using 'Nile red, nimodipine, curcumin and dexamethasone' as model dyes/drugs. Cellular uptake and enzyme-triggered release studies were also performed using Nile red as a model dye.

2. Results and discussion

The amphiphilic architectures grafted with mPEG (M_n: 550/1000 g mol^{-1}) as hydrophilic moiety and *n*-alkyl chains (C-10/C-18) conjugated with aromatic moiety as hydrophobic units, were synthesized by following the Novozym 435 catalyzed chemoenzymatic approach followed by copper catalyzed "1,3-dipolar cycloaddition reaction" (Schemes 1–3, Fig. 1). The physicochemical characterization and solubilization behavior of all the resulting amphiphiles were studied using various spectroscopic and analytical techniques, *i.e.*, NMR, IR, UV, fluorescence, gel permeation chromatography (GPC), dynamic light scattering (DLS), and surface tension measurements. The synthesized amphiphiles were also explored for their cytotoxicity profile using A549 cell lines.

2.1. Synthesis and characterization

The hydrophobic components bearing dialkyne (**9**/**10**) were synthesized following the strategy as outlined in Scheme 1

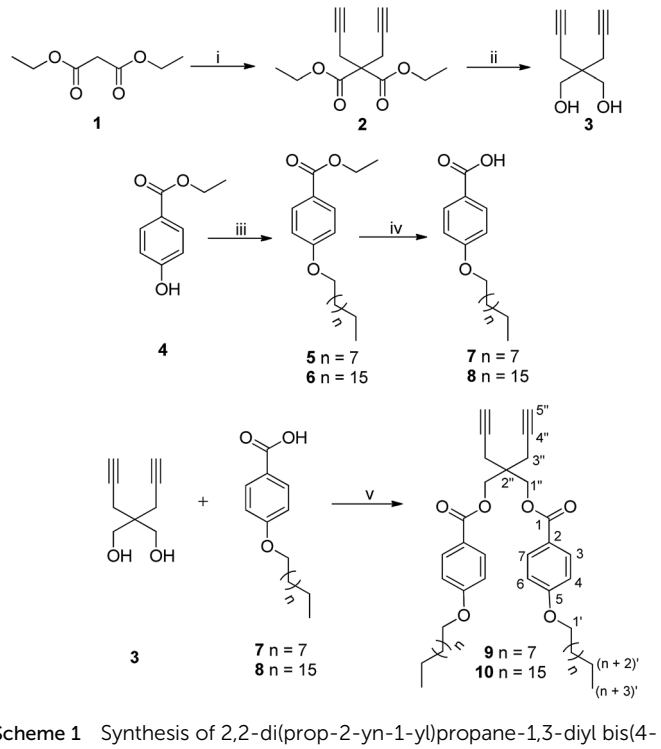

Scheme 1 Synthesis of 2,2-di(prop-2-yn-1-yl)propane-1,3-diyl bis(4-(*n*-alkyloxy)benzoate); reagents and conditions: (i) NaH, propargyl bromide, THF, 25 °C, 12 h; (ii) $LiAlH_4$, THF, 25 °C, 12 h; (iii) K_2CO_3, 1-bromoalkane, DMF, 40 °C, 6 h; (iv) KOH, ethanol, reflux, 4 h; (v) EDC, DMAP, DCM : DMF (4 : 1), 30 °C, 48 h.

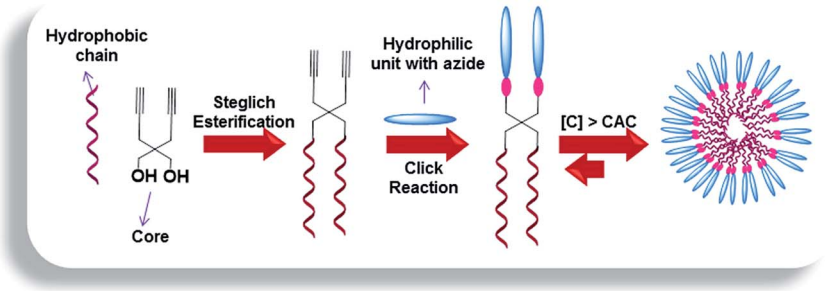

Fig. 1 Representation of synthetic approach and self-assembly of the amphiphiles in aqueous media.

using 2,2-di(prop-2-yn-1-yl)propane-1,3-diol (**3**) as the core. Dipropargylation of diethyl malonate (**1**) using sodium hydride as base afforded diethyl 2,2-di(prop-2-yn-1-yl)malonate (**2**),[37] which on reduction with lithium aluminium hydride led to the formation of compound **3**.[38] Steglich esterification was successfully carried out using the diol **3** and 4-(*n*-alkyloxy)benzoic acid (**7**/**8**) employing *N*-(3-dimethylaminopropyl)-*N*-ethylcarbodiimide hydrochloride (EDC) and 4-dimethylaminopyridine (DMAP) to yield 2,2-di(prop-2-yn-1-yl)propane-1,3-diyl bis(4-(*n*-alkyloxy)benzoate) (**9**/**10**). 4-(*n*-Alkyloxy)benzoic acid (**7**/**8**) in turn, was synthesized from ethyl 4-hydroxybenzoate (**4**) by *O*-alkylation using 1-bromoalkane followed by de-esterification in the presence of potassium hydroxide as a base and ethanol as solvent under reflux conditions (Scheme 1).[39]

2,2-Di(prop-2-yn-1-yl)propane-1,3-diyl bis(4-(*n*-alkyloxy) benzoate) (**9**/**10**) synthesized following Scheme 1 was completely characterized by IR, ^{1}H, ^{13}C NMR and HRMS. In the IR spectra of compound **9**/**10**, peak around 3280 cm^{-1} confirmed the presence of terminal alkyne group and in ^{1}H NMR spectrum, the terminal acetylenic proton appeared as a triplet at δ 2.07 ppm due to coupling with the methylene adjacent to the triple bond. The peak for the carbon at the acetylenic end was observed at around δ 72 ppm in ^{13}C NMR spectrum, however, the adjacent carbon (–C≡CH) appeared relatively downfield (δ 79 ppm). The presence of hydrophobic chains was ascertained by the appearance of triplet at δ 0.88 ppm (J = 6.9 Hz) integrating for six protons and other methylenes in δ 1.2–1.8 ppm range in ^{1}H NMR spectrum.

The synthesis of mPEG based hydrophilic motif functionalized with azide group (**18**/**19**) was successfully achieved from azido-glycerol (**17**) and mPEG ethyl ester (**15**/**16**) using a Novozym 435-catalyzed biocatalytic route under solvent-free conditions (Scheme 2). mPEG ethyl esters (**15**/**16**) were synthesized from commercially available mPEG-550 (**11**) and mPEG-1000 (**12**) in two steps. mPEG (**11**/**12**) was first oxidized to its corresponding acids (**13**/**14**) using alkaline $KMnO_4$ in aqueous media in almost quantitative yield without further purification. The mPEG-550/1000 acids (**13**/**14**) were then converted to their ethyl ester derivatives (**15**/**16**) by using a standard esterification protocol (Scheme 2).[40] Azido glycerol (**17**), used to introduce azide functionality to the hydrophilic part, was synthesized from commercially available glycerol in four steps following the protocol as reported earlier by our group.[40]

IR, ^{1}H, and ^{13}C NMR spectra were used to confirm the structure of mPEG acids (**13** and **14**). In the IR spectra of compounds **13** and **14**, appearance of an extra peak around 1700 cm^{-1} for the carboxyl group and a singlet at δ 4.14 ppm, integrating for two methylene protons adjacent to carboxyl functionality in ^{1}H NMR confirmed the oxidation of the alcoholic group. The integration ratio for the peaks of corresponding

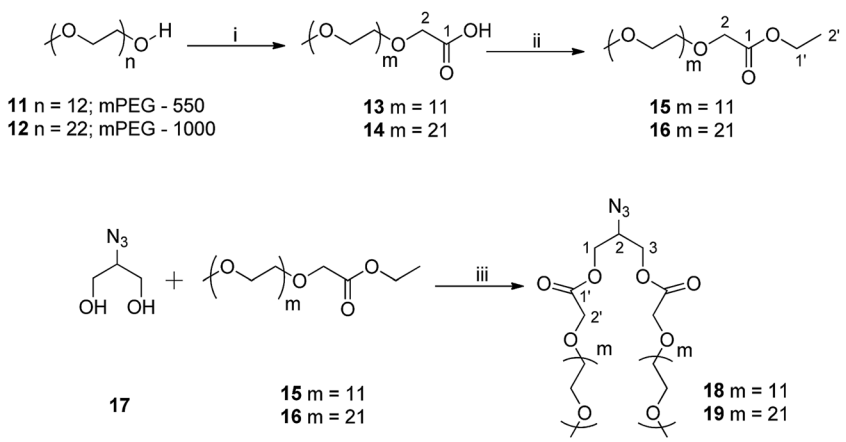

Scheme 2 Synthesis of 2-azidopropane-1,3-diyl bis(methoxypoly(oxyethylene)oate); reagents and conditions: (i) $KMnO_4$, NaOH, H_2O, 0–80 °C, 24 h; (ii) ethanol, conc. H_2SO_4 (cat.), 90 °C, 12 h; (iii) Novozym 435, 70 °C, 60 h, vacuum.

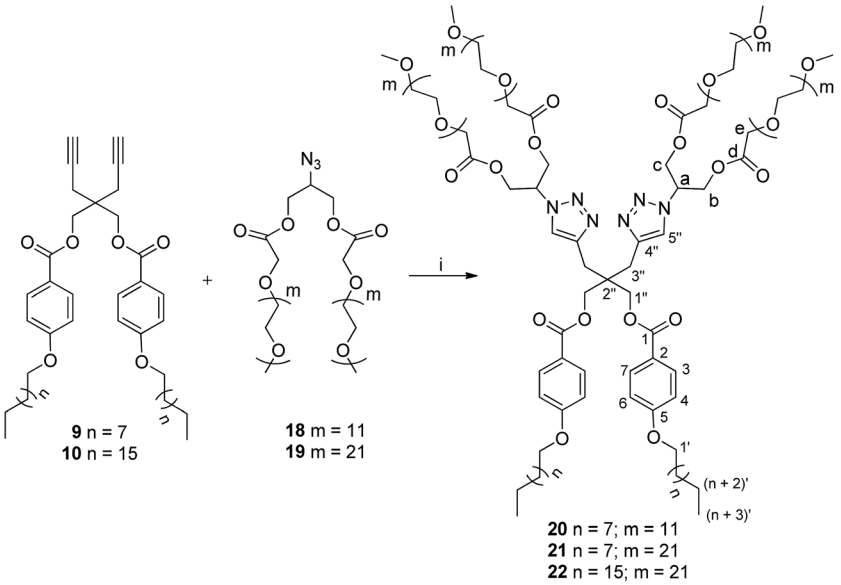

Scheme 3 Synthesis of amphiphiles; reagents and conditions: (i) $[Cu(PPh_3)_3]Br$, DIPEA, DCM, 30 °C, 72 h.

methylene protons and PEG main chain established the complete oxidation of mPEG (**11**/**12**) to mPEG acid (**13**/**14**). The peak for carboxylic carbon was also observed at around δ 171 ppm in ^{13}C NMR. Further, the formation of mPEG ethyl ester (**15**/**16**) was confirmed by the triplet around δ 1.20 ppm and quartet around δ 4.10 ppm in ^{1}H NMR spectrum integrating for three and two protons of the methyl and methylene groups of ethyl moiety, respectively. Novozym 435-catalyzed synthesis of hydrophilic scaffolds (**18**/**19**) was also characterized utilizing the spectroscopic techniques. The peak for azide group at around 2100 cm^{-1} in IR spectrum and multiplets in the range of δ 4.11–4.44 and 3.87–3.93 ppm corresponding to methylene groups of azido glycerol and the ones adjacent to the carboxyl group of mPEG, and methine of azido glycerol in the ^{1}H NMR spectrum, respectively confirmed the formation of compounds **18** and **19**. Furthermore, in the ^{13}C NMR spectrum, the methylene groups next to the carboxyl functionality and those of azido glycerol appeared at around δ 68 and 63 ppm, respectively, and the methine carbon of azido glycerol appeared at δ 58 ppm. The methoxy carbon of mPEG was observed at δ 58 ppm, relatively deshielded to the methine carbon of azido glycerol.

The different hydrophobic (**9**/**10**) and hydrophilic units (**18**/**19**) were coupled together under 'Click regime' using tris (triphenylphosphine)copper(I) bromide and DIPEA with DCM as a solvent to yield mPEG based non-ionic amphiphiles **20–22** (Scheme 3).

The completion of coupling reaction of azide functional group of hydrophilic scaffold with the alkyne functionalized hydrophobic chains leading to the formation of amphiphiles **20–22** was confirmed by the disappearance of azide peak at around 2100 cm^{-1} in the IR spectra. The formation of product was further ascertained by the observance of aromatic protons of (*n*-alkyloxy)benzoates and triazole moieties in the ^{1}H NMR spectrum. The ^{13}C NMR spectrum also supported the synthesis of desired products by the appearance of additional peaks in the aromatic region corresponding to (*n*-alkyloxy)benzoates (δ 113, 121, 131 & 162 ppm) and triazolyl ring carbons (δ 124 & 142 ppm). Furthermore, triazole ring formation also resulted in the characteristic downfield shift for the methine protons of glycerol from δ 3.86–3.94 ppm to δ 5.37–5.48 ppm in the ^{1}H NMR spectrum, which was further established from ^{2}D heteronuclear correlation (HETCOR) and correlation spectroscopy (COSY) NMR spectra (Fig. S13, ESI†). The integration ratio for the terminal methyl protons of hydrophobic chain and PEG main chain protons further confirmed the formation of the desired products.

2.2. Physico-chemical characterization of supramolecular nanostructures

All the amphiphilic systems displayed supramolecular aggregation behavior in aqueous solution (Fig. 2). The CAC of the resulting nano-structures was determined by the surface tension[20] (pendant drop method) and fluorescence measurements using pyrene[41] and Nile red[42] as probes. DLS measurements were used for determining the particle size. In order to supplement the results obtained from DLS measurements and to have an idea about the morphology of amphiphilic architectures, cryo-TEM images were also recorded.

2.2.1. Calculation of critical aggregation concentration using surface tension and fluorescence measurements. Surface tension, one of the most commonly used properties of the amphiphiles which varies consistently with the concentration until the aggregates are formed, was used for calculating the CAC in aqueous media. Once the CAC is attained, surface tension either becomes constant or changes with a lower slope. The plot of surface tension values *versus* log[amphiphile conc.] led to the observance of curve break and the amphiphile concentration at this point was referred to CAC, as exemplified in Fig. 3a and S15 (ESI†). The CAC value of the amphiphilic

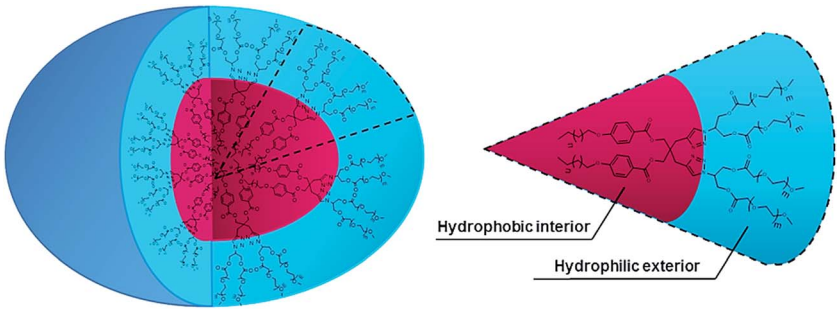

Fig. 2 Schematic representation of supramolecular aggregation of nanocarriers **20–22**.

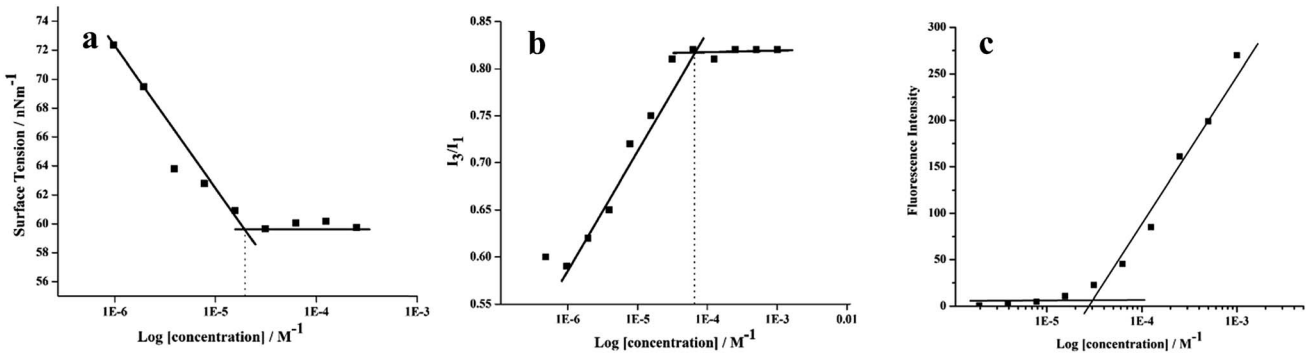

Fig. 3 Exemplary plots of (a) surface tension and (b) I_3/I_1 ratio of pyrene (c) Nile red fluorescence intensity *versus* log concentration of the amphiphile **22** in aqueous solution at 25 °C.

systems which formed stable micellar aggregates were calculated and are given in Table 1. All the amphiphiles exhibited a low CAC value ranging from 1.15×10^{-5} M to 1.96×10^{-5} M.

The CAC of an aqueous solution of self-assembled amphiphiles was also determined by calculating the ratio of the fluorescence intensity of I_3 (385 nm) and I_1 (374 nm) vibronic bands of encapsulated pyrene at different amphiphile concentrations (Fig. 3b and S16, ESI†). A correlation between the ratio of the first and third highest energy vibrational bands (I_1/I_3) of pyrene has been established with the solvent polarity.[43,44] Below the CAC, assemblies are not present, and the I_3/I_1 ratio is low, equivalent to that of pyrene in water (0.55).[45] However, with the formation of the assemblies, pyrene gets partitioned into the hydrophobic core and an increase in the I_3/I_1 ratio is observed (up to 1.66 in aliphatic hydrocarbon solvents such as hexane).[45] The CAC calculated using fluorescence method was found to be in the range of 5.77×10^{-5} M to 6.32×10^{-5} for all the synthesized amphiphiles (Table 1).

The plot of fluorescence intensity of encapsulated Nile red *versus* log[amphiphile conc.] gave the CAC value of the amphiphiles ranging from 2.69×10^{-5} M to 3.01×10^{-5} M (Table 1, Fig. 3c and S17 (ESI†)). The amphiphile **21** bearing C-10 alkyl chains as hydrophobic component and mPEG-1000 units as hydrophilic part was found to have the lowest CAC value, measured by surface tension as well as fluorescence method, however the amphiphile **22** having C-18 alkyl chains along with mPEG-1000 aggregated at a relatively higher concentration.

2.2.2. Dynamic light scattering and cryo-TEM measurements. The aggregation phenomenon of synthesized amphiphiles was also studied in aqueous medium by DLS measurements at a concentration of 5 mg mL^{-1} (Table 1). The size distribution profile was monomodal in volume and

Table 1 Physico-chemical properties of amphiphiles **20–22**

	CAC (M)			DLS (D_h, nm)		
Amphiphile	Surface tension measurement	Pyrene fluorescence measurement	Nile red fluorescence measurement	I^a	V^b	N^c
20	1.89×10^{-5}	6.24×10^{-5}	2.87×10^{-5}	10.24	7.49	6.08
21	1.15×10^{-5}	5.77×10^{-5}	2.69×10^{-5}	11.98	8.53	6.82
22	1.96×10^{-5}	6.32×10^{-5}	3.01×10^{-5}	19.32	17.49	16.07

[a] Intensity distribution. [b] Volume distribution. [c] Number distribution. DLS data was measured at 5 mg mL^{-1} concentration for all the amphiphiles.

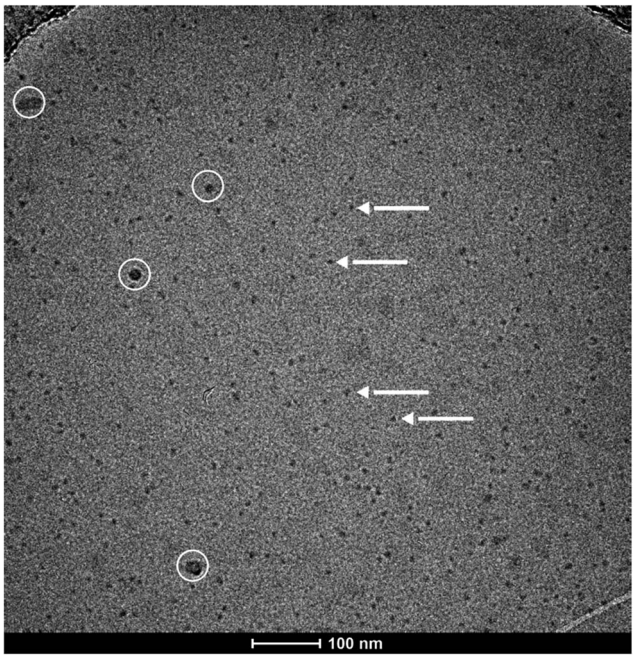

Fig. 4 Cryo-TEM image of amphiphile **22** showing micellar assembly (arrows and white circles indicate micelles and surface contamination, respectively), some of them having slightly discoidal morphology.

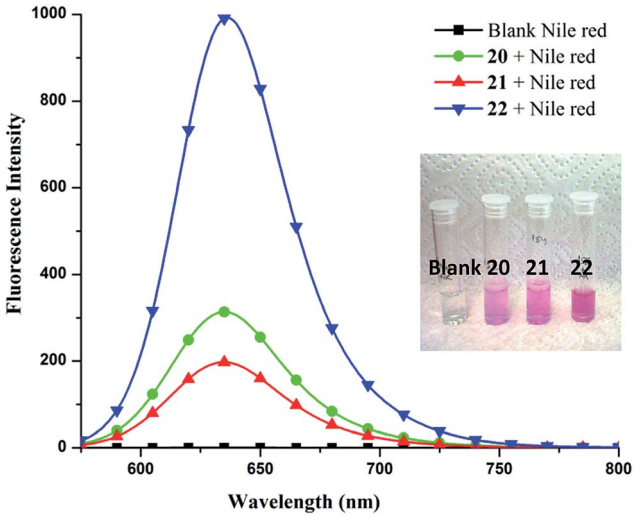

Fig. 5 Fluorescence intensity of encapsulated Nile red in the amphiphiles **20**–**22** in methanol.

number, but exhibited bimodal distribution in intensity which may be assigned to micelles and micellar aggregates (Fig. S18, ESI†). This gave an indication that the smaller size particles observable in volume and number, were the predominant species in the aqueous solution. In the light of the literature reports which state that the smaller nanoparticles in the range of 8–20 nm not only can easily penetrate the deep regions of interstitial tissue, but also circumvent the rapid renal clearance of the drugs being delivered,[46] it seemed that the size of the self-assembled system was quite appropriate for transport purposes. The estimated assembly dimensions of the dominating nano-sized species in the aqueous solution ranged from 6–19 nm and followed the order: mPEG-550; C-10 chain (**20**) < mPEG-1000; C-10 chain (**21**) < mPEG-1000; C-18 chain (**22**).

Assuming that the morphology of the particles is spherical, DLS is generally used to determine the hydrodynamic size of the particles and their distribution profile in a sample. However, the actual morphology of the nanostructures cannot be ascertained by DLS. Therefore, cryo-TEM was utilized to directly investigate the complementary morphology for compounds **20**, **21** and **22**. Fig. 4 presents a representative cryo-TEM micrograph for amphiphile **22** showing a population of micellar assemblies with a diameter of 8 nm, with some of them having discoidal morphology. In case of amphiphiles **20** and **21**, particles with diameter < 5 nm were observed (Fig. S19, ESI†), which is reasonably in agreement with DLS data given that the hydrodynamic radius of the assemblies is generally larger than the visible assembly structure, as the hydration shell does not contribute density in the cryo-TEM images (Fig. 4).

2.3. Encapsulation potential

To explore the applicability of these new non-ionic amphiphilic systems as nanocarriers, drug/dye solubilization experiments were performed. The encapsulation potential of the amphiphiles was determined for four different exemplary hydrophobic entities, the dye Nile red, and the three drugs nimodipine, curcumin and dexamethasone, all of which might interact with the nanocarriers through non-covalent interactions such as hydrophobic, π–π stacking and hydrogen bonding, employing either the film method[47] or solid dispersion method.[48] The resulting calculations of the transport efficiency, transport capacity and encapsulation efficiency are presented in Table 2. Further, to get insight into the encapsulation process, drug/dye encapsulated samples were studied by DLS which revealed that there was no significant change in size

Table 2 Transport efficiency, transport capacity and encapsulation efficiency of **20**–**22** for Nile red, nimodipine, curcumin and dexamethasone

	Transport efficiency (mg g^{-1})				Transport capacity (mmol mol^{-1})				Encapsulation efficiency[e] (%)			
Amphiphile	NR[a]	NIM[b]	CUR[c]	DXM[d]	NR	NIM	CUR	DXM	NR	NIM	CUR	DXM
20	1.12	21.03	37.89	17.33	10.86	155.28	317.87	136.47	4.66	21.03	18.95	8.67
21	0.97	8.00	26.45	12.67	14.83	93.63	351.22	157.83	4.02	8.00	13.22	6.33
22	5.79	22.86	41.66	12.67	93.03	279.33	578.16	165.06	23.33	22.86	20.83	6.33

[a] NR = Nile red. [b] NIM = nimodipine. [c] CUR = curcumin. [d] DXM = dexamethasone. [e] Encapsulation efficiency (%) = amount of dye encapsulated × 100/amount of dye added.

Table 3 Size distribution profile (by volume) of **20–22** before and after encapsulation determined by DLS measurements

		After encapsulation			
Compound	Before encapsulation	Nile Red	Curcumin	Nimodipine	Dexamethasone
20	7.49	10.31	7.57	7.76	10.06
21	8.53	12.10	9.53	9.44	9.66
22	17.49	14.75	16.04	12.72	12.29

after encapsulation of the hydrophobic guest molecules (Table 3 and Fig. S20 (ESI†)). In case of C-18 alkyl chain functionalized amphiphile **22**, slight contraction in particle size was observed upon encapsulation of dye/drug molecules. This could be attributed to greater hydrophobic interactions of encapsulated dye/drug with C-18 alkyl chain as compared to C-10 alkyl chain. Moreover, smaller assemblies formed by C-10 alkyl chain bearing amphiphiles **20** and **21** might be responsible for the observance of slight increase and no contraction in size, when hydrophobic guest molecules were encapsulated.

2.3.1. Nile red encapsulation. Nile red, a model hydrophobic and solvatochromic fluorescent dye, is very commonly used for evaluating the transport potential and local polarity of nanocarriers.[49] H- and J-type aggregates which are known to be formed by Nile red beyond a certain concentration, is marked by an additional shoulder peak in the absorption spectra and a change in the fluorescence intensity.[50] As reported earlier by our group, 0.12 mg of the dye with 5 mg mL^{-1} of nanocarrier solution resulted in monomolecular and maximum encapsulation of the chromophore determined by fluorescence measurements.[51,52] In order to further ascertain this for our systems, fluorescence intensity measurements were carried out by varying the amount of Nile red and the amphiphile (**20**) concentration, which revealed that maximum fluorescence was observed for 0.12 mg of chromophore with 5 mg mL^{-1} of amphiphile (Fig. S21†). Thus, we decided to use 5 mg mL^{-1} of amphiphile concentration and 0.12 mg of Nile red for encapsulation to avoid the formation of aggregates. Further, the same concentration (5 mg mL^{-1}) of the amphiphile was used for all other encapsulation studies.

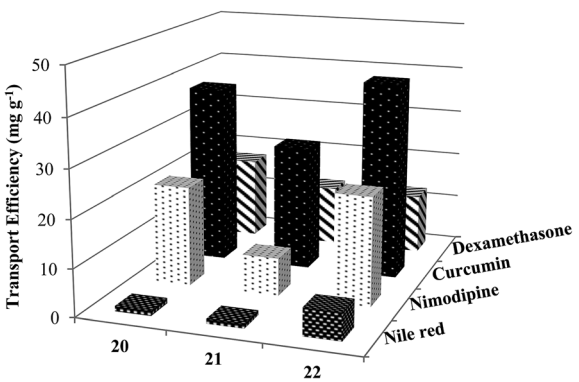

Fig. 6 Guest transport efficiencies (mg g^{-1}) for amphiphiles **20–22**.

To quantify Nile red encapsulation, lyophilization of the encapsulated samples followed by dissolution in methanol was carried out with subsequent recording of their absorbance and fluorescence emission spectra. The transport efficiency (Fig. 6) and transport capacity (Table 2) of the encapsulated dye was calculated for all the amphiphiles employing the Beer–Lambert's law and using the molar extinction coefficient (ε) of 45 000 M^{-1} cm^{-1} at 552 nm.[53] The amphiphile **22** consisting of mPEG-1000 and C-18 alkyl chains showed the maximum encapsulation followed by amphiphiles **20** and **21** (transport efficiency; **20:** 1.12 mg g^{-1}, **21:** 0.97 mg g^{-1}, **22:** 5.79 mg g^{-1}), which was also supported by fluorescence measurements (Fig. 5). Further, comparison of transport and encapsulation efficiency of amphiphile **22** with aromatic and non-aromatic polymeric systems synthesized earlier by our group revealed that this system (**22**) possessed superior solubilization behavior.[51,52,54]

2.3.2. Nimodipine encapsulation. Nimodipine, a 1,4-dihydropyridine calcium channel blocker with therapeutic indications for cerebrovascular spasm, stroke, migraine, and ischemic neurological disorders, has restricted clinical usefulness due to low oral bioavailability and aqueous solubility.[55] In this regard, nanoparticles hold substantial promise and thus, we attempted to entrap the drug in the amphiphilic architectures (**20–22**) at an amphiphile concentration of 5 mg mL^{-1}. Absorbance measurements of the encapsulated samples at different drug concentration (0.2, 0.5 and 1 mg) (Fig. S23, ESI†) propelled us to use 0.5 mg of nimodipine with quantitative estimation achieved using a molar extinction coefficient of the drug in ethanol (7200 M^{-1} cm^{-1} at 356 nm).[20] Amphiphile **22** having greater hydrophobic core exhibited highest encapsulation efficiency as it could efficiently transport 22.86 mg of nimodipine for 1 g of **22** (Fig. 6).

2.3.3. Curcumin encapsulation. Enriched with profound therapeutic properties, curcumin finds myriad applications such as anticancer, antimicrobial, antioxidant and anti-inflammatory agent.[54] Curcumin having a biphenolic structure, has been a promising candidate for the treatment of Alzheimer's disease as it binds to amyloid plaques in *in vivo* and prevents the aggregation of Aβ into fibrils.[56] However, low aqueous solubility together with high chemical and photochemical instability leading to poor bioavailability, confines its use as drug.[54] In an attempt to enhance its bioavailability, we have successfully encapsulated curcumin using our amphiphilic systems (**20–22**). Encapsulation and quantitative evaluation was assessed from UV-Vis spectrophotometry at two different drug concentrations (1 and 2.5 mg) and 5 mg mL^{-1}

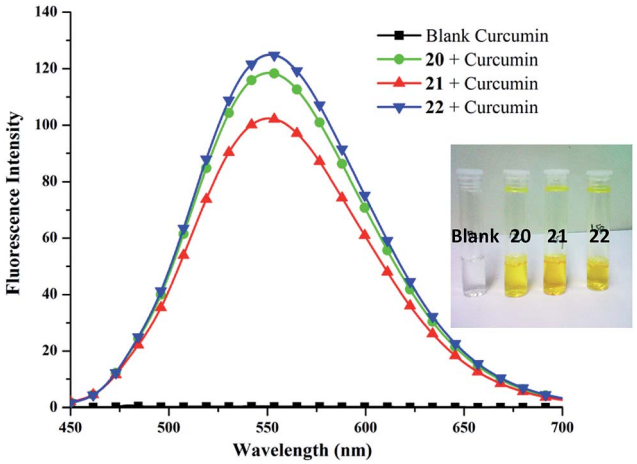

Fig. 7 Fluorescence intensity of encapsulated curcumin in the amphiphiles **20–22** in methanol.

amphiphile solution using a molar extinction coefficient of the drug in methanol (55 306 M^{-1} cm^{-1} at 425 nm), obtained from calibration curve (Fig. S25, ESI†). Highest encapsulation was observed when 1 mg of curcumin along with 5 mg mL^{-1} of amphiphile was used (Fig. S26, ESI†). In a 5 mg mL^{-1} solution of nanocarriers **20–22**, it was possible to solubilize 132.2–208.2 mg L^{-1} of curcumin; thus, enhancing its solubility in water at 25 °C by approximately 10^4 times from ~11 ng mL^{-1} as reported in literature.[57]

Furthermore, amphiphile **22** was found to be the best candidate as 1 g of it could uptake 41.66 mg of curcumin, followed by amphiphiles **20** and **21**, which could transport 37.89 and 26.45 mg of curcumin respectively (Fig. 6). This observation was further supplemented by fluorescence measurements (Fig. 7). This suggests the attainment of an optimum balance between hydrophobic and hydrophilic units in the amphiphile **22** for curcumin encapsulation. It has been observed that the formulation of curcumin/amphiphile in 1 : 5 ratio (w/w) led the C-18 alkyl containing amphiphile **22** to encapsulate higher percentage of curcumin as compared to the C-18 alkyl functionalized PEGylated copolymers employing 1 : 2 curcumin/polymer ratio (Table 4).[48] Moreover, the synthesized amphiphiles **20–22** using 1 : 5 and 1 : 2 formulation ratio were found to possess superior transport efficiency, transport capacity and % encapsulation efficiency as compared to the alkyl and perfluoroalkyl-functionalized dendronized polymers synthesized earlier by our group,[58] wherein 1 : 3 curcumin/polymer ratio was used (Table 4). Furthermore, Rabanel *et al.*[59] also used 1 : 5 loading ratio for PEG–poly lactic acid (PLA) polymers (PEG 8%-*g*-PLA, PEG 20%-*g*-PLA, PEG-*b*-PLA and OH-*g*-PLA) but reported lower % transport and encapsulation efficiency than our system, with the exception of PEG 8%-*g*-PLA (Table 4). In addition, the % encapsulation efficiency of amphiphile **22** was found to be comparable to the $mPEG_{2000}$–oleic acid (OA) diblock copolymer, however, the % transport efficiency was ~1.5 fold lower in our case (Table 4).[60]

2.3.4. Dexamethasone encapsulation. In order to further investigate the suitability of these novel amphiphilic nanocarriers (**20–22**) as possible drug delivery systems, we tried to exploit the poor aqueous soluble corticoid, dexamethasone. Endowed with anti-inflammatory properties, dexamethasone has been used for the treatment of diabetic macular edema.[61] Analysis of the encapsulated samples at two different drug concentrations (1 and 2.5 mg) and 5 mg mL^{-1} of nanocarrier solution (Fig. S27 and S28, ESI†) *via* HPLC using acetonitrile : water mixture (40 : 60) as an eluent, led to the observance of best transportation while using 1 mg of the drug. Since, dexamethasone has partial solubility in water, therefore, a blank sample was prepared wherein the drug was stirred in water without the amphiphile. From the results, it was inferred that unlike the outcomes for Nile red, nimodipine and curcumin where compound **22** had the highest transport efficiency, 1 g of the nanocarrier having C-10 alkyl chain decorated with mPEG-550 (**20**) successfully transported 17.33 mg of dexamethasone. On the other hand, amphiphiles **21** and **22** exhibited lower transport efficiency of 12.67 mg g^{-1} (Fig. 6). This

Table 4 Comparison of % transport efficiency, transport capacity and % encapsulation efficiency of **20–22** for curcumin with that of the nanocarriers reported in literature

Nanocarrier	Curcumin/nanocarrier ratio (w/w)	Transport efficiency (%)	Transport capacity (mmol mol^{-1})	Encapsulation efficiency (%)
20	1 : 2	2.28	279.92	4.57
21	1 : 2	2.11	191.69	4.21
22	1 : 2	2.29	317.97	4.58
20	1 : 5	3.79	317.87	18.95
21	1 : 5	2.65	351.22	13.22
22	1 : 5	4.17	578.16	20.83
Stearyl polymer[48]	1 : 2	—	—	15.41
Stearoyl polymer[48]	1 : 2	—	—	9.26
50% perfluoroalkyl-functionalized dendronized polymers[58]	1 : 3	0.53	213.17	1.6
70% perfluoroalkyl-functionalized dendronized polymers[58]	1 : 3	0.45	176.75	1.4
50% alkyl-functionalized dendronized polymers[58]	1 : 3	0.27	98.95	0.8
70% alkyl-functionalized dendronized polymers[58]	1 : 3	0.39	135.41	1.2
PEG–PLA polymer[59]	1 : 5	<2	—	</= 10
PEG 8%-*g*-PLA polymer[59]	1 : 5	5	—	15
$mPEG_{2000}$–OA polymer[60]	1 : 5	~6	—	~20

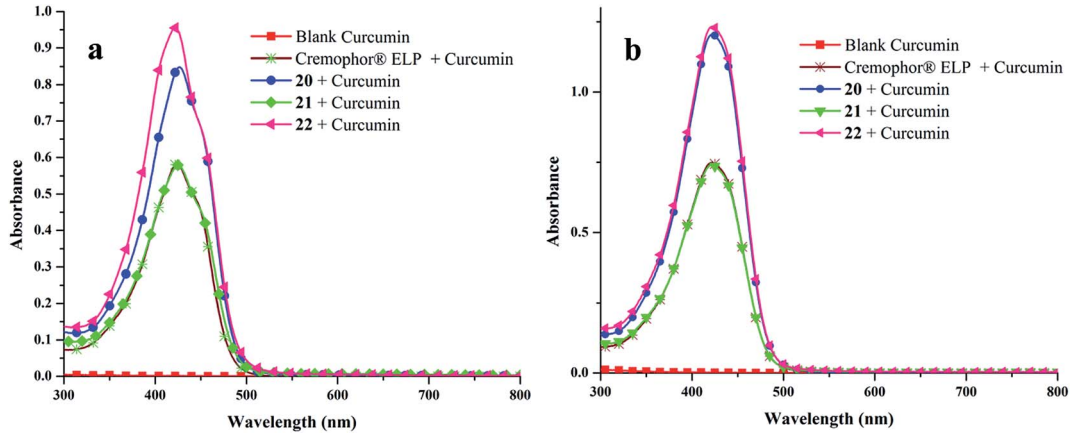

Fig. 8 Absorbance spectra of encapsulated curcumin in the amphiphiles **20**–**22** and Cremophor® ELP in (a) water and (b) methanol.

might be due to the presence of a carboxylic group in dexamethasone which renders it slight hydrophilic character. Moreover, higher dexamethasone carrying ability of the synthesized nanocarriers **20**–**22** was observed on comparison with those of perfluoroalkyl-functionalized dendronized polymers reported earlier by our group.[58]

It was of interest to note the correlation between the CAC of a nanotransporter with its dye/drug loading capacity; in fact, amphiphile **22** allowed to encapsulate approximately 1.6–6 times more dye/drug, in most cases, than the nanocarrier **21**. Nevertheless, it was possible to confirm the fundamental importance of the hydrophobicity of the micellar core from the results collected, that allowed the formation of relatively larger aggregates (amphiphile **22**), and ultimately enabling high dye/drug solubilization.

2.3.5. Comparison with Cremophor® ELP. Among all the dyes/drugs screened for their encapsulation behavior, curcumin was found to be the best candidate in terms of its solubilization efficiency and capacity (Fig. 6). Therefore, in pursuit of a comparative study of our developed amphiphilic systems (**20**–**22**) with a standard excipient, Cremophor® ELP was used. Absorbance spectra measurements were carried out at a concentration of 1 mg for curcumin and 5 mg mL^{-1} for compounds **20**–**22** and Cremophor® ELP. As presented in Fig. 8, amphiphiles with relatively appropriate hydrophobic–hydrophilic balance (**20**/**22**) possessed a remarkably higher solubilization for curcumin compared with the standard excipient used. On the other hand, nanocarrier with mPEG-1000 and C-10 alkyl chain (**21**) had comparable drug loading tendency.

2.4. Cellular uptake study

The cellular internalization of Nile red encapsulated in two selected amphiphiles **20** and **22** having different hydrophilic and hydrophobic ratios in A549 lung cancer cells was studied by confocal laser scanning microscopy (cLSM).

The Nile red encapsulated supramolecular architectures were prepared by incubating the dye in an aqueous solution of amphiphile using the film method at a concentration of 5 mg mL^{-1}. The cLSM images (Fig. 9) revealed that the dye encapsulated in amphiphiles **20** and **22** could be internalized into the cells. After 5 h, a strong signal was seen in the cytosol and in

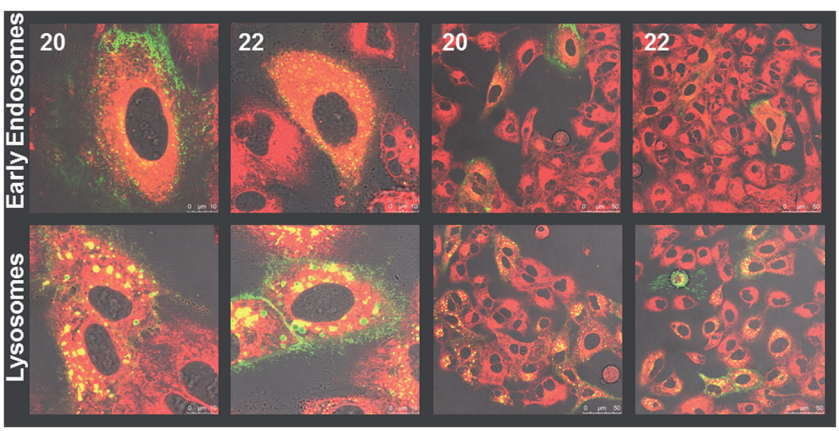

Fig. 9 Confocal laser scanning fluorescence microscopy images from A549 cells after 5 h incubation with Nile red encapsulated by amphiphiles **20** and **22**. In the images, Nile red is shown in red color, labeled early endosomes and lysosomes in green. Yellow color indicates a merge of green and red color and therefore shows co-localization of Nile red and early endosomes or lysosomes. The bright field channel is shown in grey scale.

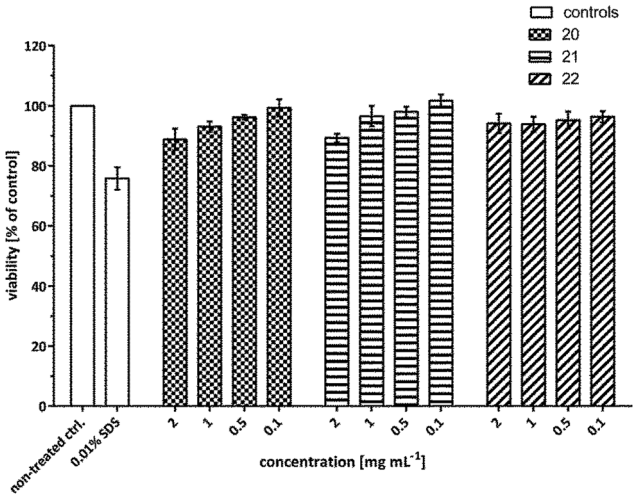

Fig. 10 Cytotoxicity profile of amphiphiles (**20–22**) after 24 h. Cytotoxicity of the nano-carriers was determined by an MTS assay in A549 cells 24 h post-treatment. Each bar represents the mean value of three independent experiments ($n = 3$) measured in triplicates with SEM.

some lysosomes. Further, it was observed that the fluorescence intensity was increasing over time indicating a continuous uptake of the encapsulated dye and accumulation (Fig. S29, ESI†). The labeled and non-labeled control cells showed no fluorescence in the Nile red channel (Fig. S29, ESI†).

2.5. Cytotoxicity

In order to develop efficient nanocarriers for biomedical applications such as drug delivery, the cytotoxicity is one of the major areas of concern that needs to be addressed. Therefore, to examine the *in vitro* cytotoxicity of the synthesized amphiphilic systems, A549 cells were treated with the compounds **20–22** at a concentration of 2, 1, 0.5 and 0.1 mg mL^{-1} and the viability was assayed using MTS assay after 24 h.

The cytotoxicity profile unveiled that all the developed systems exhibited nearly no cytotoxicity even up to the highest concentration tested. Though, amphiphiles **20** and **21** exhibited marginal toxicity of ~10% at 2 mg mL^{-1}, however, nanocarrier **22** containing C-18 alkyl chain was found to be non-cytotoxic at this concentration even up to 24 h post-treatment (Fig. 10).

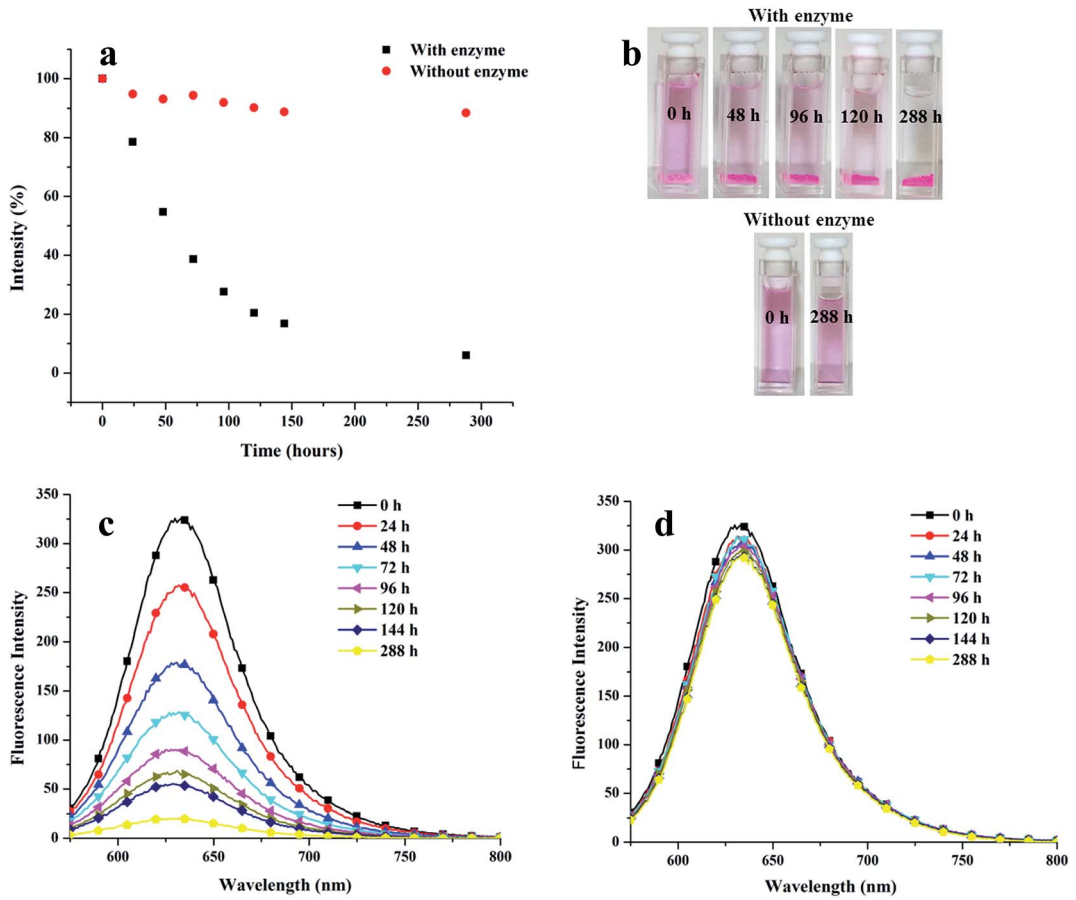

Fig. 11 (a) Release profile of Nile red encapsulated nanocarrier **22** under physiological conditions, in the presence and absence of enzyme at 37 °C; (b) time dependent release of Nile red from amphiphile **22** with/without enzyme; (c) fluorescence intensity of encapsulated Nile red in the presence of enzyme; (d) fluorescence intensity of encapsulated Nile red in the absence of enzyme.

2.6. Enzyme-triggered release study

The release of encapsulated drug in a controlled manner to maintain its therapeutic concentration holds great relevance apart from its encapsulation. Since the amphiphiles reported herein contain ester linkages that might be sensitive to enzyme catalyzed hydrolytic conditions, Novozym 435 mediated cleavage of Nile red encapsulated nanocarrier **22** was performed under dark conditions. Fig. 11 presents the time-dependent decay of fluorescence intensity maximum of Nile red-loaded amphiphile **22** under physiological conditions in the presence and absence of the enzyme.

The intensity of the pink colour of the Nile red encapsulated solution diminished with time when the nanocarrier was placed in an environment similar to the human body, in the presence of the enzyme. Approximately 50% decay in the intensity occurred after 54 h and it was possible to have more than 80% release only after 120 h (Fig. 11). Interestingly, the dye encapsulated nanocarrier under physiological conditions in the absence of the enzyme was observed to be fairly stable; in fact insignificant amount of Nile red was released from the system adopting such conditions.

3. Conclusions

Herein, we have reported a "greener" chemo-enzymatic method which has been deployed to synthesize non-ionic amphiphiles from biocompatible starting materials, *i.e.*, mPEG and glycerol, by grafting different alkyl chains and mPEG on a dipropargylated propane-1,3-diol core. All the amphiphilic systems have the tendency to form supramolecular aggregates in aqueous solution with CAC in the order of 10^{-5} M and DLS size in the range of 6–19 nm. Cryo-TEM study of the amphiphiles led to the conclusion of formation of micellar assemblies. An enhancement in the encapsulation potential has been observed with increase in the hydrophobic content of the amphiphilic systems as the amphiphile constituted from C-18 alkyl chain and mPEG 1000 has the highest transport efficiency for Nile red, nimodipine and curcumin as compared to the other synthesized amphiphiles. However, in case of dexamethasone, mPEG 550 and C-10 alkyl chain containing architecture exhibited maximum solubilization behavior. Moreover, the encapsulation of hydrophobic entities did not result in a significant change in the size. A comparison of the synthesized nanocarriers with standard excipient revealed that the developed systems have higher or equivalent solubilization for curcumin. Efficient uptake of encapsulated dye in the cytosol and lysosomes of lung cancer cells was shown by confocal microscopy indicating, that the amphiphilic systems can transport drugs into cells. More interestingly, the cytotoxicity profile obtained from MTS assay unraveled that the synthesized amphiphilic architectures showed negligible cytotoxicity at the tested concentrations, which is relevant for drug delivery systems. The enzyme-triggered release profile of the encapsulated dye revealed that approximately 50% decay in the fluorescence intensity occurred after 54 h in the presence of the enzyme with more than 90% release taking place in 12 days. In contrast, the control having no enzyme showed insignificant Nile red release. Thus, it could be concluded from the results obtained here that a balance between hydrophobicity and hydrophilicity plays a key role for the amphiphilic architectures to act as good nanotransporters. This study may facilitate further development of optimized amphiphiles as nanocarriers for biomedical applications.

Acknowledgements

We gratefully acknowledge the financial assistance from SERB-DST, Government of India and University of Delhi. Also, we are thankful to CSIR, New Delhi, for providing fellowship to Suchita Prasad.

References

1 C. Branden and J. Tooze, *Introduction to protein structure*, Garland Publishing Inc., New York, 2nd edn, 1999.
2 M. Lee, B. K. Cho and W. C. Zin, *Chem. Rev.*, 2001, **101**, 3869–3892.
3 V. Percec, A. E. Dulcey, V. S. K. Balagurusamy, Y. Miura, J. Smidrkal, M. Peterca, S. Nummelin, U. Edlund, S. D. Hudson, P. A. Heiney, H. Duan, S. N. Magonov and S. A. Vinogradov, *Nature*, 2004, **430**, 764–768.
4 M. A. Alam, Y. S. Kim, S. Ogawa, A. Tsuda, N. Ishii and T. Aida, *Angew. Chem., Int. Ed.*, 2008, **47**, 2070–2073.
5 J. A. A. W. Elemans, A. E. Rowan and R. J. M. Nolte, *J. Mater. Chem.*, 2003, **13**, 2661–2670.
6 S. I. Stupp and L. C. Palmer, *Chem. Mater.*, 2014, **26**, 507–518.
7 B. Wang, H. Xu and X. Zhang, *Adv. Mater.*, 2009, **21**, 2849–2864.
8 N. Kamaly, Z. Xiao, P. M. Valencia, A. F. Radovic-Moreno and O. C. Farokhzad, *Chem. Soc. Rev.*, 2012, **41**, 2971–3010.
9 Y. B. Lim, K. S. Moon and M. Lee, *Chem. Soc. Rev.*, 2009, **38**, 925–934.
10 Y. Liu, B. Liu and Z. Nie, *Nano Today*, 2015, **10**, 278–300.
11 S. Gupta, R. Tyagi, V. S. Parmar, S. K. Sharma and R. Haag, *Polymer*, 2012, **53**, 3053–3078.
12 V. P. Torchilin, *Cell. Mol. Life Sci.*, 2004, **61**, 2549–2559.
13 H. Gelderblom, J. Verweij, K. Nooter and A. Sparreboom, *Eur. J. Cancer*, 2001, **37**, 1590–1598.
14 A. J. ten Tije, J. Verweij, W. J. Loos and A. Sparreboom, *Clin. Pharmacokinet.*, 2003, **42**, 665–685.
15 C. Tanford, *The hydrophobic effect. Formation of micelles and biological membranes*, Wiley-Interscience, New York, 2nd edn, 1980, p. 233.
16 M. Ramanathan, L. K. Shrestha, T. Mori, Q. Ji, J. P. Hill and K. Ariga, *Phys. Chem. Chem. Phys.*, 2013, **15**, 10580–10611.
17 A. Sorrenti, O. Illa and R. M. Ortuno, *Chem. Soc. Rev.*, 2013, **42**, 8200–8219.
18 M. Malmsten, *Soft Matter*, 2006, **2**, 760–769.
19 X. Zhang and C. Wang, *Chem. Soc. Rev.*, 2011, **40**, 94–101.
20 B. N. S. Thota, H. V. Berlepsch, C. Böttcher and R. Haag, *Chem. Commun.*, 2015, **51**, 8648–8651.
21 F. Bordi, G. Cerichelli, N. D. Berardinis, M. Diociaiuti, L. Giansanti, G. Mancini and S. Sennato, *Langmuir*, 2010, **26**, 6177–6183.

22 L. Shi, F. Chen, N. Sun and L. Zheng, *Soft Matter*, 2015, **11**, 4075–4080.
23 W. Zhao and Y. Wang, *Adv. Colloid Interface Sci.*, 2017, **239**, 199–212.
24 R. Santhana, G. Krishnan, S. Thennarasu and A. B. Mandal, *J. Phys. Chem. B*, 2004, **108**, 8806–8816.
25 H. C. Kim, E. Kim, S. G. Lee, S. J. Lee, H. Kim and S. W. Jeong, *J. Polym. Sci., Part A: Polym. Chem.*, 2014, **52**, 582–589.
26 S. Sen, R. Schowner, D. A. Imbrich, W. Frey, M. Hunger and M. R. Buchmeiser, *Chem.–Eur. J.*, 2015, **21**, 13778–13787.
27 M. Guo, R. Sun, H. Han, J. Wu, M. Xie and X. Liao, *Macromolecules*, 2015, **48**, 2378–2387.
28 M. Sudheendran, M. Horecha, A. Kiriy, S. A. Gevorgyan, F. C. Krebs and M. R. Buchmeiser, *Polym. Chem.*, 2013, **4**, 1590–1599.
29 E. H. Kang and T. L. Choi, *ACS Macro Lett.*, 2013, **2**, 780–784.
30 Y. H. Kim, D. C. Shin, C. S. Ha, W. J. Cho and S. K. Kwon, *J. Polym. Sci., Part A: Polym. Chem.*, 1999, **37**, 4135–4139.
31 H. H. Fox, M. O. Wolf, R. O'Dell, B. L. Lin, R. R. Schrock and M. S. Wrighton, *J. Am. Chem. Soc.*, 1994, **116**, 2827–2843.
32 E. H. Kang, I. S. Lee and T. L. Choi, *J. Am. Chem. Soc.*, 2011, **133**, 11904–11907.
33 P. S. Kumar, K. Wurst and M. R. Buchmeiser, *J. Am. Chem. Soc.*, 2009, **131**, 387–395.
34 S. Das, S. Mandal, B. Mukhopadhyay and S. S. Zade, *Tetrahedron Lett.*, 2012, **53**, 1464–1467.
35 T. H. Ali, R. S. D. Hussen and T. Heidelberg, *Colloids Surf., B*, 2014, **123**, 981–985.
36 B. Trappmann, K. Ludwig, M. R. Radowski, A. Shukla, A. Mohr, H. Rehage, C. Böttcher and R. Haag, *J. Am. Chem. Soc.*, 2010, **132**, 11119–11124.
37 S. Das, A. Bedi, G. R. Krishna, C. M. Reddy and S. S. Zade, *Org. Biomol. Chem.*, 2011, **9**, 6963–6972.
38 L. Q. Xu, F. Yao and G. D. Fu, *Macromolecules*, 2009, **42**, 6385–6392.
39 X. Y. Hu, K. Jia, Y. Cao, Y. Li, S. Qin, F. Zhou, C. Lin, D. Zhang and L. Wang, *Chem.–Eur. J.*, 2015, **21**, 1208–1220.
40 S. Gupta, B. Schade, S. Kumar, C. Böttcher, S. K. Sharma and R. Haag, *Small*, 2013, **9**, 894–904.
41 A. C. Greene, J. Zhu, D. J. Pochan, X. Jia and K. L. Kiick, *Macromolecules*, 2011, **44**, 1942–1951.
42 A. C. Rodrigo, A. Barnard, J. Cooper and D. K. Smith, *Angew. Chem., Int. Ed.*, 2011, **50**, 4675–4679.
43 O. Colombani, M. Ruppel, F. Schubert, H. Zettl, D. V. Pergushov and A. H. E. Müller, *Macromolecules*, 2007, **40**, 4338–4350.
44 I. Astafieva, X. F. Zhong and A. Eisenberg, *Macromolecules*, 1993, **26**, 7339–7352.
45 R. K. Kainthan, C. Mugabe, H. M. Burt and D. E. Brooks, *Biomacromolecules*, 2008, **9**, 886–895.
46 V. P. Torchilin, *Nat. Rev. Drug Discovery*, 2005, **4**, 145–160.
47 E. Fleige, B. Ziem, M. Grabolle, R. Haag and U. Resch-Genger, *Macromolecules*, 2012, **45**, 9452–9459.
48 V. Kumar, B. Gupta, G. Kumar, M. K. Pandey, E. Aiazian, V. S. Parmar, J. Kumar and A. C. Watterson, *J. Macromol. Sci., Pure Appl. Chem.*, 2010, **47**, 1154–1160.
49 M. Wyszogrodzka and R. Haag, *Chem.–Eur. J.*, 2008, **14**, 9202–9214.
50 I. N. Kurniasih, H. Liang, S. Kumar, A. Mohr, S. K. Sharma, J. P. Rabe and R. Haag, *J. Mater. Chem. B*, 2013, **1**, 3569–3577.
51 M. Kumari, S. Gupta, K. Achazi, C. Böttcher, J. Khandare, S. K. Sharma and R. Haag, *Macromol. Rapid Commun.*, 2015, **36**, 254–261.
52 M. Kumari, A. K. Singh, S. Kumar, K. Achazi, S. Gupta, R. Haag and S. K. Sharma, *Polym. Adv. Technol.*, 2014, **25**, 1208–1215.
53 R. P. Haugland, *Handbook of Fluorescent Probes and Research Chemicals*, Molecular Probes Inc., Eugene, OR, USA, 6th edn, 1996.
54 M. Kumari, M. Billamboz, E. Leonard, C. Len, C. Böttcher, A. K. Prasad, R. Haag and S. K. Sharma, *RSC Adv.*, 2015, **5**, 48301–48310.
55 G. M. Soliman, R. Sharma, A. O. Choi, S. K. Varshney, F. M. Winnik, A. K. Kakkar and D. Maysinger, *Biomaterials*, 2010, **31**, 8382–8392.
56 J. M. Ringman, S. A. Frautschy, E. Teng, A. N. Begum, J. Bardens, M. Beigi, K. H. Gylys, V. Badmaev, D. D. Heath, L. G. Apostolova, V. Porter, Z. Vanek, G. A. Marshall, G. Hellemann, C. Sugar, D. L. Masterman, T. J. Montine, J. L. Cummings and G. M. Cole, *Alzheimer's Res. Ther.*, 2012, **4**, 43–50.
57 M. H. Ucisik, S. Küpcü, B. Schuster and U. B. Sleytr, *J. Nanobiotechnol.*, 2013, **11**, 37–49.
58 B. Parshad, M. Kumari, K. Achazi, C. Böttcher, R. Haag and S. K. Sharma, *Polymers*, 2016, **8**, 311–325.
59 J. M. Rabanel, J. Faivre, G. D. Paka, C. Ramassamy, P. Hildgen and X. Banquy, *Eur. J. Pharm. Biopharm.*, 2015, **96**, 409–420.
60 A. M. Alizadeh, M. Sadeghizadeh, F. Najafi, S. K. Ardestani, V. Erfani-Moghadam, M. Khaniki, A. Rezaei, M. Zamani, S. Khodayari, H. Khodayari and M. A. Mohagheghi, *BioMed Res. Int.*, 2015, **2015**, 824746.
61 C. Gómez-Gaetea, N. Tsapis, M. Besnard, A. Bochot and E. Fattal, *Int. J. Pharm.*, 2007, **331**, 153–159.